

Breakdown of traditional many-body theories for correlated electrons

O. Gunnarsson,¹ G. Rohringer,² T. Schäfer,³ G. Sangiovanni,⁴ and A. Toschi³

¹ *Max-Planck-Institut für Festkörperforschung, Heisenbergstraße 1, D-70569 Stuttgart, Germany*

² *Russian Quantum Center, Novaya street, 100, Skolkovo, Moscow region 143025, Russia*

³ *Institute of solid state physics, Vienna University of Technology, 1040 Vienna, Austria*

⁴ *Institute of Physics and Astrophysics, University of Würzburg, Würzburg, Germany*

(Dated: November 7, 2018)

Starting from the (Hubbard) model of an atom, we demonstrate that the uniqueness of the mapping from the interacting to the noninteracting Green's function, $G \rightarrow G_0$, is strongly violated, by providing numerous explicit examples of different G_0 leading to the same physical G . We argue that there are indeed *infinitely* many such G_0 , with numerous crossings with the physical solution. We show that this rich functional structure is directly related to the divergence of certain classes of (irreducible vertex) diagrams, with important consequences for traditional many-body physics based on diagrammatic expansions. Physically, we ascribe the onset of these highly non-perturbative manifestations to the progressive suppression of the charge susceptibility induced by the formation of local magnetic moments and/or RVB states in strongly correlated electron systems.

PACS numbers: 71.10.-w; 71.27.+a; 71.10.Fd

Introduction. For more than fifty years non-relativistic quantum many-body theory (QMBT) has been successfully applied to describe the physics of many-electron systems in the field of condensed matter. Despite the intrinsic difficulty of identifying a small expansion parameter (analogously to the the fine-structure constant of quantum-electrodynamics), the formalism of QMBT –in its complementary representations in terms of Feynman diagrammatics[1, 2] and of the universal Luttinger-Ward (LW) functional[3, 4]– is the cornerstone of the microscopic derivation of Landau's Fermi-liquid theory and of uncountable approximation schemes[5–9].

Yet, the actual conditions of applicability of the QMBT in the non-perturbative regime have been scarcely investigated. This is surprising, because QMBT is extensively applied to strongly correlated electron materials, where band-theory and Fermi-liquid predictions fail, and some of the most exotic physics of condensed matter systems is observed. Recently, however, the quest for such investigations became particularly strong. This is because several cutting-edge QMBT-approaches, explicitly designed for describing the crucial, but elusive, regime of intermediate-to-strong interactions, have been developed, e.g., the diagrammatic Quantum Monte Carlo (DQMC) schemes [10] and numerous diagrammatic extensions[11–16] of dynamical mean field theory (DMFT) [9, 17].

Pioneering analyses of the perturbation theory breakdown have been reported in the last four years[18–27]. The main outcome can be summarized in two independent observations: (i) the occurrence of *infinitely* many singularities in the Bethe-Salpeter equations and (ii) the intrinsic multivaluedness of the LW functionals. The first problem appears as an infinite series of unexpected *divergences* in irreducible vertex functions [19], while the second is reflected in the convergence of the perturbative series to an unphysical solution[20]. The intrinsic origin

of these non-perturbative manifestations, their impact on the many-electron physics, as well as on the method development in the field, represent a challenge for the current theoretical understanding.

In this Letter, we report a fundamental progress in the comprehension of the perturbation theory breakdown and of its significance. In particular, going beyond the pioneering work of [20], (i) we show that there are many (probably an infinite number of) unphysical self-energies that become equal to the physical one at specific values of the interaction. This puts us into the position to (ii) demonstrate the actual correspondence between the vertex divergences of the Feynman diagrammatics and the occurrence of bifurcations of the LW functional. Finally, (iii) we generalize these results from the Hubbard atom to generic systems with strong correlations. Regarding the nature of the singularities, we show that vertex divergences of different kinds are reflected in different natures of solution crossings at the bifurcation.

The emerging scenario, which *mathematically* depicts an unexpectedly complex structure of the many-body formalism, will be *physically* related to the progressive suppression of charge fluctuations, a generic property of strongly-correlated systems with a local interaction. The improved understanding of the QMBT beyond the perturbative regime serves as a crucial guidance for future method development for non-relativistic many-electron systems.

Multivaluedness of the Luttinger-Ward functional. The Luttinger-Ward (LW) functional $\Phi[G]$ plays a crucial role in traditional many-body physics [4]. It is a universal functional of the full single-particle Green's function G , which only depends on the electron-electron interaction but not on the external potential. From $\Phi[G]$ the free energy can be determined. One can also obtain the electron self-energy $\Sigma[G] \sim \delta\Phi[G]/\delta G$, entering the Dyson

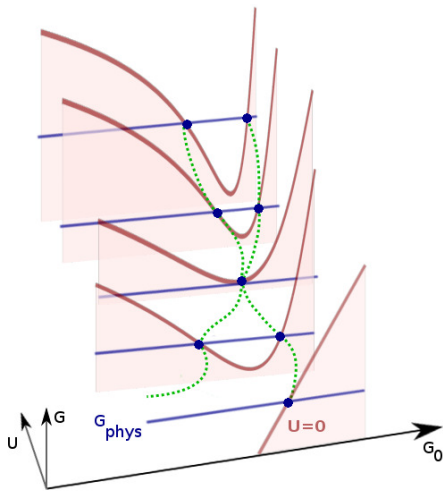


FIG. 1: Sketch of the functional $G[G_0, U]$, where G_0 and G are assumed to be just numbers: The red curves correspond to cuts for different values of U , the horizontal blue lines show the corresponding values of G_{phys} , while the blue dots represent the G_0 which produce G_{phys} .

equation

$$G_0^{-1} - G^{-1} = \Sigma, \quad (1)$$

where G_0 is the noninteracting Green's function determined by the external potential. From $\Sigma[G]$ one can compute all irreducible vertices Γ entering the Bethe-Salpeter equations [8] for response functions. For instance, the charge susceptibility is determined by the vertex [3, 8, 19, 20]

$$\Gamma_c = \frac{\delta \Sigma[G]}{\delta G}. \quad (2)$$

Approximations built within this approach are guaranteed to be conserving [3], therefore it is exploited for numerous formal derivations [9, 29–31]. Moreover, the full two-particle nature of the vertices Γ represents an ideal building block for approximations designed to preserve the Pauli principle properties, and related sum rules. In this respect, it is believed that the parquet equations [8] are one of the most fundamental ways of performing diagrammatic summations.

In order for QMBT methods to be meaningful, an important property of the functional $G[G_0]$ needs to be fulfilled: The introduction of Σ in QMBT implicitly assumes that there is a unique mapping between G and G_0 , $G \rightarrow G_0$. Otherwise, several branches of Σ would exist, corresponding to different G_0 , posing the general problem of an intrinsic multivaluedness of any QMBT-based scheme. This is not just a formal issue. If two such branches cross, Γ in Eq. (2) might become ill-defined and diverge. This would challenge important aspects of the traditional many-body theory, such as, e.g., the definition of physically meaningful parquet summations [32].

Fig. 1 schematically illustrates such a scenario. The general functional relation between G and G_0 is depicted by several red curves for different values of the electronic interaction U [33]. G and G_0 are here treated as numbers rather than functions (of frequency/momentum/spin, etc.). For $U = 0$, $G[G_0] = G_0$, and for any physical G (horizontal blue line) the corresponding G_0 is *univocally* determined. When $U > 0$, however, $G[G_0]$ becomes “wavier”, displaying several maxima/minima in the functional space. This way, the intersection with G_{phys} would correspond to several G_0 (blue dots), of which only one describes the physical system (G_0^{phys}). Even if unphysical G_0 's exist, many standard numerical algorithms are able to converge to the solution that is adiabatically connected with the $U = 0$ one. This can however turn into an actual problem, *if* for some values of U the intersection with G_{phys} occurs at one extreme of $G[G_0]$. This would correspond to the intersection of two different solutions of G_0 (and thus of Σ , see green dashed lines in Fig. 1). At this point we would expect $\delta G/\delta G_0 = 0$. Combining this with the Dyson equation and the definition [Eq. (2)] of Γ_c , one would conclude that Γ_c diverges.

To go beyond the sketch of Fig. 1, we present calculations for the Hubbard atom [34] and show that different G_0 indeed do cross for certain values of U . In Sec. IA of the Supplemental Material [28] we then show that such a crossing indeed does lead to divergences of Γ_c .

Method. We have developed a method for finding different G_0 's which lead to the physical G for the Hubbard atom. We use the Hirsch-Fye algorithm [35] to obtain G from a guess for G_0 . This method involves a summation over auxiliary spins, which is usually done stochastically. Here we perform a complete summation using the Gray code [36], thereby avoiding stochastic errors. We guess a G_0 , and then use a Metropolis method to search for improved guesses for G_0 . When a promising guess has been found, the Hirsch-Fye equations are repeatedly linearized and solved, until a G_0 has been found which accurately reproduces the physical G (see Sec. II of [28]). It is crucial that there are no stochastic errors in this approach. The method makes it possible to determine if two G_0 really become equal for some U and to determine how they approach each other as U is varied.

Results for the Hubbard atom. We start to present our results by showing in Fig. 2 (left panel) $\text{Tr} \Sigma G_{\text{phys}}/(\beta U)$ as a function of U corresponding to the different G_0 and, hence Σ , via Eq. (1). For $G_0 = G_0^{\text{phys}}$, this quantity yields the double occupancy. The black curve displays the values obtained with $G_0 = G_0^{\text{phys}}$, while the colored (red, orange) curves are the results for the other (unphysical) G_0 , collapsing to G_0^{phys} in the several crossing points shown in the Figure. The latter ones *do* coincide -within our numerical accuracy- with the locations (marked by vertical arrows) of the first six divergences of Γ_c in the Hubbard atom [19]. The red G_0 's are associ-

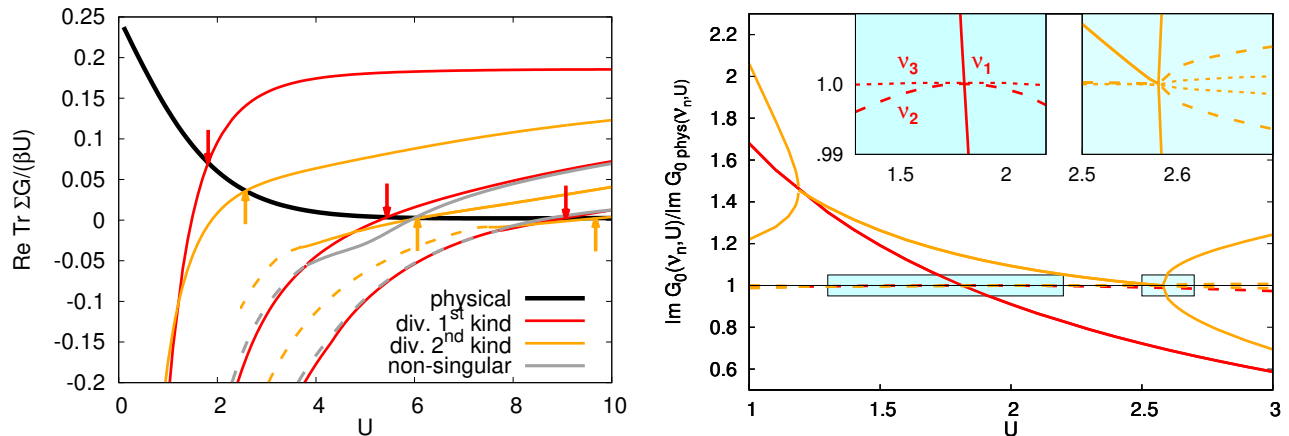


FIG. 2: Left: $\text{Tr } \Sigma G/(\beta U)$ as a function of U corresponding to different G_0 for the Hubbard atom for $\beta = 2$. Red/orange arrows mark the divergences of Γ_c according to Ref. [19]. The physical curve corresponding to G_0^{phys} is shown in black. Beyond the red/orange ones, one finds further crossings (gray lines) for which, however, $G_0(\nu) \neq G_0^{\text{phys}}(\nu)$ and, hence no divergence of Γ_c is found (see Sec. IC of the Supplemental Material [28]). Dashed curves indicate that $\text{Tr } \Sigma G/(\beta U)$ also has an imaginary contribution, which is not shown. Right: imaginary part of G_0 (normalized to $\text{Im } G_0^{\text{phys}}$) for the first red and orange curves. Results for the absolutely lowest (bold lines), second lowest (dashed lines) and (in insets) third lowest (dotted lines) ν_n are shown.

ated with a milder violation of physical constraints than the orange ones (e.g., the former can acquire a non-zero real part, but the latter can even violate the generic condition: $G_0(\nu) = G_0(-\nu)^*$ [28]). The left red curve was found by Kozik *et al.* [20], although, there, it could not be converged around the crossing with G_0^{phys} .

There are important connections between the frequency dependence of the divergences of Γ_c , coded by red/orange colors [19], and the detailed behavior of G_0 at a crossing. The divergences of Γ_c can be divided into two classes [18, 19]. To this end, we consider the generalized charge susceptibility $\chi_c^{\nu\nu'(\omega=0)}$ [37], which depends on two fermionic Matsubara frequencies, ν and ν' , and a bosonic frequency $\omega = 0$. Γ_c is then given by

$$\Gamma_c = \beta^2 [\chi_c^{-1} - \chi_0^{-1}], \quad (3)$$

where χ_0 is the noninteracting generalized susceptibility χ_c , and χ_c and $\chi_{c,0}$ are treated as matrices of ν and ν' . These matrices can be diagonalized

$$\chi_c^{\nu\nu'(\omega=0)} = \sum_l V_l(\nu)^* \varepsilon_l V_l(\nu'), \quad (4)$$

with $V_l(\nu)$ and ε_l being the corresponding eigenvectors/-values. While the divergences of Γ_c always correspond to the vanishing of one ε_l , they differ in the frequency-structure of $V_l(\nu)$: For the divergences marked by the red arrows, $V_l(\nu)$ has only two non-zero elements (at $\nu = \pm\nu_n = \pm(2n-1)\pi/\beta$, with $n = 1, 2, 3, \dots$) reflecting a *local* divergence at $\nu = \pm\nu_n$, while for the orange arrows, $V_l(\nu) \neq 0 \forall \nu$, reflecting a *global* divergence of Γ_c [19].

An analogous classification is also applicable to the different G_0 resolved in frequency space: In Fig. 2b we plot the ratio $\text{Im } G_0(\nu)/\text{Im } G_0^{\text{phys}}(\nu)$ corresponding to the first two crossings and for the three lowest ν . As G_0^{phys} is purely imaginary, the condition $G_0(\nu) = G_0^{\text{phys}}(\nu)$ is reflected in their ratio being 1 and $\text{Re } G_0/\text{Im } G_0^{\text{phys}} = 0$ (shown in Supplemental Material [28]). Fig. 2b demonstrates that the red/orange crossings observed in $\text{Tr } \Sigma G_{\text{phys}}$ indeed corresponds to an actual identity of $G_0(\nu) = G_0^{\text{phys}}(\nu)$, $\forall \nu$ both at $U = 1.81$ (red) and 2.58 (orange). Yet, the corresponding zooms in the insets show a *qualitative* difference between the two cases. For the red case, the crossing of G_0 with G_0^{phys} is *linear* in U only for $\nu = \pi/\beta$ (solid line), while it is $O(U^2)$ for all other ν_n (dashed line). In the orange case, the crossings display the *same* behavior for all the frequencies (see insets of Fig. 2 and the discussion in Sec. IA of [28]). This leads to a divergence of Γ_c for $\nu, \nu' = \pm\pi/\beta$ at the red crossing and for all frequencies at the orange crossing. Similar results are found for the second and third red/orange crossings, but for the former the linear crossing happens for $\nu_2 = 3\pi/\beta$ (second) and $\nu_3 = 5\pi/\beta$ (third). This is consistent with the result in Ref. [19] that the corresponding divergences of Γ_c happens at these specific ν_n .

The one-to-one correspondence of red/orange crossings with the local/global divergences of Γ_c illustrates how the heuristic scenario of Fig. 1 is actually realized for the Hubbard atom. The result also indicates the existence of an *infinite* number of unphysical G_0 , since *infinitely* many red and orange divergences were found for the Hubbard atom [19]. Furthermore, there are indications that the

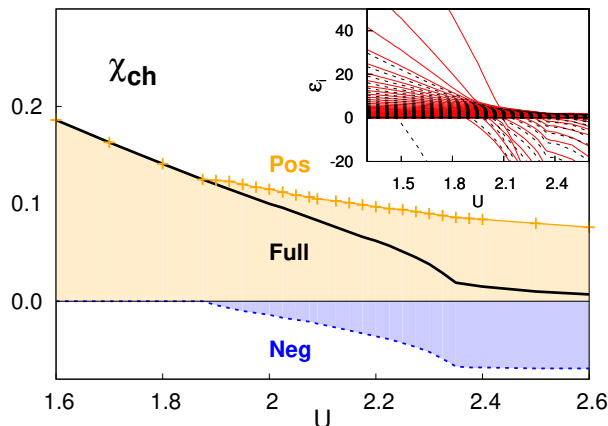


FIG. 3: DMFT calculation of the local charge susceptibility (χ_{ch}) [Eq. (5)] (black line) as a function of U for a two-dimensional Hubbard model at half-filling, $\beta = 40$ and $4t = 1$. Both χ_{ch} and its contributions from positive (orange) and negative (blue) eigenvalues are shown. The inset shows the U -dependence of the eigenvalues ε_i , using solid lines for ε_i with $\sum_{\nu} V_l(\nu) \neq 0$ and dashed lines for the rest.

infinity of the total number of G_0 might be of a higher cardinality than that of the vertex divergences, as we discuss in Sec. III of the Supplemental Material [28].

Generic strongly correlated systems. – To make closer contact to strongly correlated physical systems, we consider the Hubbard model in DMFT [9, 17], where the Hubbard atom is embedded in a self-consistent, noninteracting host. The LW functional is unchanged, since it only depends on the interacting part of the Hamiltonian. The external-potential part, however, changes, and therefore both G_{phys} and G_0^{phys} are different. We can exploit the relation of the crossings with the divergences of Γ_c and the zero eigenvalues in Eq. (4), and gain further insight by analyzing the physical local charge susceptibility. In DMFT, this is given by [32]

$$\chi_{\text{ch}} = \frac{1}{\beta^2} \sum_{\nu\nu'} \chi_c^{\nu,\nu'}(\omega=0) = \frac{1}{\beta^2} \sum_l \varepsilon_l \left| \sum_{\nu} V_l(\nu) \right|^2. \quad (5)$$

The corresponding DMFT results are reported in Fig. 3. By increasing U , the electrons gradually localize, building up local magnetic moments with longer lifetimes. These, in turn, freeze the local charge dynamics, with χ_{ch} becoming very small especially in the proximity/after the Mott metal-insulator transition (between $U = 2.3$ and $U = 2.4$ for $\beta = 40$). While the physics of this generic trend is known, the projection of χ_{ch} in its eigenvalue-basis yields highly non-trivial information. We analyze χ_{ch} in terms of the contributions from positive and negative ε_l . For small/moderate U all ε_l are positive. As U increases, one ε_l after the other goes through zero (see inset of Fig. 3). Each time Γ_c diverges [see Eqs. (3, 4)], a new G_0 becomes identical to G_0^{phys} ,

and the negative component of χ_{ch} becomes more important. Such a negative component of χ_{ch} plays a crucial role in realizing the correct strong coupling physics. Its neglect would lead to a χ_{ch} approximately saturating at some sizable value in the Mott phase, instead of being strongly suppressed. We also note, that a small value of χ_{ch} in itself is not sufficient for this scenario to be realized (e.g., in a dilute system χ_{ch} can be small, but all $\varepsilon_l > 0$). Here, the crucial factor is the mechanism responsible for the reduction of χ_{ch} : the gradual local moment formation which manifests itself in a progressively larger contribution of the negative ε_l . This is, thus, the underlying physics responsible for the occurrence of the (infinitely many) unphysical G_0 crossing G_0^{phys} , and the related divergences of Γ_c . This also applies to the corresponding breakdown of perturbative expansions, such as parquet-based approximations. A certain class of diagrams can give a positive infinite contribution, which is canceled by another class of diagrams [32]. Then the diagrammatic expansion is not absolutely convergent, as was also found in Ref. [20]. This makes conventional diagrammatic expansions highly questionable for intermediate-to-strong correlations. While it is not surprising that perturbative approaches might break down at the Mott transition, it is interesting that this happens well before the Mott transition occurs, where Fermi-liquid physical properties still control the low-energy physics.

It is important to stress that the non-perturbative manifestations discussed in this Letter are affecting not *only* models dominated by purely local physics (such as the Hubbard atom or its DMFT version). In fact, divergences of Γ_c have also been found [32] studying the $2d$ Hubbard model, by means of the dynamical cluster approximation (DCA) [30]. In this case, the underlying physics behind the change of sign of the ε_l could be related to the formation of an RVB state [38], also responsible [39] for the opening of a spectral pseudogap [40]. Increasing the size of the DCA cluster might even push the occurrence of the first $\varepsilon_l = 0$ and the pseudogap towards lower U , due to strong antiferromagnetic fluctuation extended on larger length scales [32, 41, 42].

Conclusions. – We have reported important progress towards the understanding of the mathematical structures of quantum many body theories in the non-perturbative regime, and of the physics behind them. The structure of the LW functionals is even richer than the pioneering work by Kozik *et al.* suggested [20]: We find a very large, probably *infinite*, number of noninteracting G_0 leading to the same dressed G . This can be regarded as a formal problem, as long as the unphysical and physical G_0 do not intersect, as it is the case in the perturbative regime. However, in the nonperturbative regime we find many crossings. These crossings reflect the analytical structure of the LW functional for physical systems. We show that they lead to divergences of irreducible vertex functions. This challenges current quan-

tum many-body algorithms in several respects, e.g., causing non-invertibility of the Bethe-Salpeter equation and breakdown of the parquet resummations. These problems, which occur when the correlation is still substantially weaker than in a Mott insulator, are, nonetheless, originated in underlying strong-coupling physical mechanisms, e.g. the formation of local moments and RVB states. This is reflected in the progressive suppression of the charge susceptibility in correlated systems. Further investigations of the theoretical foundations beyond the perturbative regime should play a central role for future method developments in condensed matter physics.

Acknowledgments. – We thank S. Ciuchi, P. Thunström, M. Capone, S. Andergassen and K. Held for insightful discussions and P. Chalupa also for carefully reading the manuscript. The authors would like to thank all attendees to the Workshop “Multiple Solutions in Many-Body Theories” held in Paris the 13th and 14th of June 2016 for interesting discussions. We acknowledge support from FWF through the projects I-2794-N35 (TS, AT) and from the research unit FOR 1346 of the DFG (GS).

-
- [1] A. A. Abrikosov, L. P. Gorkov (Author), F. A. Davis, *Methods of Quantum Field Theory in Statistical Physics* (Dover, New York, 1963).
- [2] A. L. Fetter and J. D. Valecka, *Quantum theory of many-particle systems*, McGraw Hill, New York, 1971.
- [3] G. Baym and L. P. Kadanoff, *Phys. Rev.* **124**, 287 (1961).
- [4] J. M. Luttinger and J. C. Ward, *Phys. Rev.* **118**, 1417 (1960).
- [5] L. Hedin and S. Lundqvist, *Solid State Physics* **23**, 1 (1969).
- [6] N. E. Bickers and D. J. Scalapino, *Phys. Rev. Lett.* **62**, 961 (1989).
- [7] W. Metzner, M. Salmhofer, C. Honerkamp, V. Meden, and K. Schönhammer *Rev. Mod. Phys.* **84**, 299 (2012).
- [8] For a review, see, e.g., N. E. Bickers, *Int. J. Mod. Phys. B* **5**, 253 (1991) and in *Theoretical Methods for Strongly Correlated Electrons*, edited by D. Senechal, A. Tremblay, and C. Bourbonnais (Springer-Verlag, New York, 2004), chapter 6.
- [9] A. Georges, G. Kotliar, W. Krauth, and M. Rozenberg, *Rev. Mod. Phys.* **68**, 13 (1996).
- [10] K. Van Houcke, E. Kozik, N. Prokof'ev, and B. Svistunov, in *Computer Simulation Studies in Condensed Matter Physics XXI*, edited by D. Landau, S. Lewis, and H. Schuttler (Springer Verlag, Berlin, 2008); E. Kozik, K. V. Houcke, E. Gull, L. Pollet, N. Prokof'ev, B. Svistunov, and M. Troyer, *Europhys. Lett.* **90**, 10004 (2010).
- [11] A. Toschi, A. A. Katanin, and K. Held, *Phys. Rev. B* **75**, 045118 (2007).
- [12] A. N. Rubtsov, M. I. Katsnelson, and A. I. Lichtenstein, *Phys. Rev. B* **77**, 033101 (2008).
- [13] A. N. Rubtsov, M. I. Katsnelson, and A. I. Lichtenstein, *Ann. Phys.* **327**, 1320 (2012).
- [14] G. Rohringer, A. Toschi, H. Hafermann, K. Held, V. Anisimov, and A. Katanin, *Phys. Rev. B* **88**, 115112 (2013).
- [15] T. Ayrál, and O. Parcollet, *Phys. Rev. B* **92**, 115109 (2015); T. Ayrál, and O. Parcollet, *Phys. Rev. B* **93**, 235124 (2016).
- [16] T. Ayrál, and O. Parcollet, *Phys. Rev. B* **94**, 075159 (2016).
- [17] W. Metzner and D. Vollhardt, *Phys. Rev. Lett.* **62**, 324 (1989); M. Jarrell, *Phys. Rev. Lett.* **69**, 168 (1992).
- [18] T. Schäfer, G. Rohringer, O. Gunnarsson, S. Ciuchi, G. Sangiovanni, and A. Toschi, *Phys. Rev. Lett.* **110**, 246405 (2013).
- [19] T. Schäfer, S. Ciuchi, M. Wallerberger, P. Thunström, O. Gunnarsson, G. Sangiovanni, G. Rohringer, and A. Toschi, *Phys. Rev. B* **94**, 235108 (2016).
- [20] E. Kozik, M. Ferrero, and A. Georges, *Phys. Rev. Lett.* **114**, 156402 (2015).
- [21] V. Janiš and V. Pokorny, *Phys. Rev. B* **90**, 045143 (2014).
- [22] T. Ribic, G. Rohringer, and K. Held, *Phys. Rev. B* **93**, 195105 (2016).
- [23] A. Stan, P. Romaniello, S. Rigamonti, L. Reining and J.A. Berger *New J. of Physics* **17** 093045 (2015).
- [24] R. Rossi and F. Werner, *J. Phys. A* **48**, 485202 (2015).
- [25] G. Lani, P. Romaniello, and L. Reining, *New J. Phys.* **14**, 013056 (2012).
- [26] R. Rossi, F. Werner, N. Prokof'ev, and B. Svistunov, *Phys. Rev. B* **93**, 161102(R) (2016).
- [27] W. Tarantino, P. Romaniello, J. A. Berger, and L. Reining, arXiv:1703.05587 (2017).
- [28] Supplemental Material accessible at ...
- [29] J. M. Luttinger, *Phys. Rev.* **124**, 1153 (1960).
- [30] T. Maier, M. Jarrell, T. Pruschke, and M. H. Hettler, *Rev. Mod. Phys.* **77**, 1027 (2005).
- [31] L. Pollet, N. V. Prokof'ev, and B. V. Svistunov, *Phys. Rev. B* **83**, 161103 (2011); S. Biermann, F. Aryasetiawan, and A. Georges, *Phys. Rev. Lett.* **90**, 086402 (2003).
- [32] O. Gunnarsson, T. Schäfer, J.P.F. LeBlanc, J. Merino, G. Sangiovanni, G. Rohringer, and A. Toschi, *Phys. Rev. B* **93**, 245102 (2016).
- [33] Actually, this representation corresponds to the so-called one-point model, see, e.g. [23–26].
- [34] J. Hubbard, *Proc. Roy. Soc. London A* **276**, 238 (1963); M. C. Gutzwiller, *Phys. Rev. Lett.* **10**, 159 (1963); J. Kanamori, *Progr. Theor. Phys.* **30**, 275 (1963).
- [35] J. E. Hirsch and R. M. Fye, *Phys. Rev. Lett.* **56**, 2521 (1986).
- [36] F. Gray, *Pulse code communication*, March 17, 1953 (filed Nov. 1947). U.S. Patent 2,632,058; C. D. Miller, (2000). *Binary Numbers and the Standard Gray Code. Mathematical Ideas (9 ed) Ch. 4* (Addison Wesley Longman, 2000), ISBN 0-321-07607-9.
- [37] G. Rohringer, A. Valli, and A. Toschi, *Phys. Rev. B* **86**, 125114 (2012).
- [38] P. W. Anderson, *Science* **235**, 1196 (1987); S. Liang, B. Doucot, and P. W. Anderson, *Phys. Rev. Lett.* **61**, 365 (1988).
- [39] J. Merino and O. Gunnarsson, *J. Phys.: Cond. Matter. (Fast Track Commun.)* **25**, 052201 (2013); *Phys. Rev. B* **89**, 245130 (2014).
- [40] T. Timusk and B. Statt, *Rep. Prog. Phys.* **62**, 61 (1999).
- [41] T. Schäfer, F. Geles, D. Rost, G. Rohringer, E. Arrigoni, K. Held, N. Blümer, M. Aichhorn, and A. Toschi, *Phys. Rev. B* **91**, 125109 (2015).
- [42] O. Gunnarsson, T. Schäfer, J. P. F. LeBlanc, E. Gull,

J. Merino, G. Sangiovanni, G. Rohringer, and A. Toschi,
Phys. Rev. Lett. **114**, 236402 (2015).

Breakdown of traditional many-body theories for correlated electrons –Supplemental Material–

O. Gunnarsson,¹ G. Rohringer,^{2,3} T. Schäfer,² G. Sangiovanni,⁴ and A. Toschi²

(Dated: April 7, 2017)

I. RELATION BETWEEN DIVERGENCES OF IRREDUCIBLE VERTICES AND MULTIPLE G_0

A. Analytic analysis

In this Section we show that the crossing between the physical G_0 and a nonphysical G_0 in Figs. 2 and 3 of the main text is directly related to divergences of the irreducible charge vertex Γ_c and zero eigenvalues of the corresponding generalized charge susceptibility χ_c observed in Ref. 1. In particular, we will demonstrate that the different ways how the G_0 's cross at a given interaction strength $U=U_0$ can be unambiguously related to the two types of vertex divergences (localized vs. global) found in Refs. 1 and 2 (see also Eq. (4) in the main text and the discussion below it).

Let us start by considering a generating functional for the one-particle Green's function and the susceptibility of our system³

$$\begin{aligned} \mathcal{F}[G_0^{-1}; U, \nu] &= \frac{1}{\mathcal{Z}[G_0; U]} \int D[c^+, c] c_{\nu\sigma}^+ c_{\nu\sigma} \exp \left[\right. \\ &\quad \left. \sum_{\nu'\sigma'} G_0^{-1}(\nu') c_{\nu'\sigma'}^+ c_{\nu'\sigma'} - U \int_0^\beta d\tau c_{\tau\uparrow}^+ c_{\tau\uparrow} c_{\tau\downarrow}^+ c_{\tau\downarrow} \right], \\ \mathcal{Z}[G_0^{-1}; U] &= \int D[c^+, c] \exp \left[\right. \\ &\quad \left. \sum_{\nu'\sigma'} G_0^{-1}(\nu') c_{\nu'\sigma'}^+ c_{\nu'\sigma'} - U \int_0^\beta d\tau c_{\tau\uparrow}^+ c_{\tau\uparrow} c_{\tau\downarrow}^+ c_{\tau\downarrow} \right], \end{aligned}$$

where we have assumed SU(2) symmetry, i.e., \mathcal{F} and \mathcal{Z} do not depend on the spin σ . Evaluating \mathcal{F} at the physical G_0 yields the interacting Green's functions of the system:

$$G(\nu) = \mathcal{F}[G_0^{-1}; U, \nu]. \quad (1)$$

The functional derivative of $\mathcal{F}[G_0^{-1}; U, \nu]$ w.r.t. $G_0^{-1}(\nu')$ on the other hand gives rise to the generalized charge susceptibility $\chi_c^{\nu\nu'(\omega=0)}$:

$$\chi_c^{\nu\nu'(\omega=0)} = \frac{\delta \mathcal{F}[G_0^{-1}; U, \nu]}{\delta G_0^{-1}(\nu')} \quad (2)$$

We now consider two non-interacting Green's functions $G_0^{(1)}$ and $G_0^{(2)}$ which yield the same G and cross at $U=U_0$, which implies $1/G_0^{(1)}(\nu) - 1/G_0^{(2)}(\nu) = 0$ for all Matsubara frequencies ν at $U=U_0$.

In the next step we formally express $\mathcal{F}[1/G_0^{(2)}; U, \nu]$ in terms of a (functional) Taylor expansion of \mathcal{F} around

$1/G_0^{(1)}(\nu)$:

$$\begin{aligned} \mathcal{F}[1/G_0^{(2)}; U, \nu] &= \mathcal{F}[1/G_0^{(1)}; U, \nu] + \sum_{\nu'} \frac{\delta \mathcal{F}[G_0^{-1}; U, \nu]}{\delta G_0^{-1}(\nu')} \\ &\times \left[1/G_0^{(2)}(\nu') - 1/G_0^{(1)}(\nu') \right] + O \left[\left(1/G_0^{(2)} - 1/G_0^{(1)} \right)^2 \right]. \end{aligned} \quad (3)$$

Since both $G_0^{(1)}$ and $G_0^{(2)}$ yield (by definition) the same G (for all values of U) we have $\mathcal{F}[1/G_0^{(2)}; U, \nu] = \mathcal{F}[1/G_0^{(1)}; U, \nu] = G(\nu)$. Considering, moreover, the definition of the generalized susceptibility in Eq. (2) we can express Eq. (3) as

$$\begin{aligned} \sum_{\nu'} \chi_c^{\nu\nu'(\omega=0)} \left[1/G_0^{(2)}(\nu') - 1/G_0^{(1)}(\nu') \right] \\ = O \left[\left(1/G_0^{(2)} - 1/G_0^{(1)} \right)^2 \right]. \end{aligned} \quad (4)$$

We now turn our attention to the U -dependence of this equation for U values close to U_0 where $G_0^{(1)}$ and $G_0^{(2)}$ cross. Our numerical results in Fig. 2 in the main text (Fig. 1 in this Supplemental Material) show that this crossing follows a power law behavior, i.e., $1/G_0^{(2)}(\nu) - 1/G_0^{(1)}(\nu) \sim (U - U_0)^{\eta_\nu}$ for $U \rightarrow U_0$ where the (real and positive) coefficient η_ν can be different for different Matsubara frequencies ν . This observation can be expressed, more formally, as

$$\lim_{U \rightarrow U_0} \frac{1/G_0^{(2)}(\nu) - 1/G_0^{(1)}(\nu)}{(U - U_0)^{\eta_\nu}} = \text{const} (\neq 0), \quad (5)$$

where $\eta_\nu > 0$ for all Matsubara frequencies ν and the constant on the r.h.s. of the equation can be different for different ν . Let us now consider the smallest among all η_ν , i.e.,

$$\eta^* = \text{Min}_\nu [\eta_\nu]. \quad (6)$$

We divide both sides of Eq. (4) by $(U - U_0)^{\eta^*}$ and take the limit $U \rightarrow U_0$. The r.h.s. of this equation then vanishes as it is of at least quadratic order in $1/G_0^{(2)} - 1/G_0^{(1)}$ and, hence, goes to zero as $(U - U_0)^{\eta^*}$ for $U \rightarrow U_0$. On the l.h.s. of Eq. (4) $\chi_c^{\nu\nu'(\omega=0)}$ takes just its value at $U = U_0$ while $1/G_0^{(2)}(\nu) - 1/G_0^{(1)}(\nu)$ yields a finite value $V(\nu)$ for Matsubara frequencies ν where $\eta_\nu = \eta^*$ and $V(\nu) = 0$ when $\eta_\nu > \eta^*$. Hence, Eq. (4) transforms into the following eigenvector equation

$$\sum_{\nu'} \chi_c^{\nu\nu'(\omega=0)} V(\nu') = 0. \quad (7)$$

for χ_c for the eigenvalue 0 with the eigenvector

$$V(\nu) = \lim_{U \rightarrow U_0} \frac{1/G_0^{(2)}(\nu) - 1/G_0^{(1)}(\nu)}{(U - U_0)^{\eta^*}}. \quad (8)$$

According to Refs. 1 and 2 and the discussion below Eq. (4) in the main text such vanishing eigenvalue is related to a divergence of the irreducible charge vertex Γ_c . The way *how* Γ_c diverges (local vs. global) is given by the structure of the corresponding eigenvector $V(\nu)$: a divergence of Γ_c occurs at frequencies ν where $V(\nu) \neq 0$. According to the above discussion these are exactly the frequencies where $1/G_0^{(2)}(\nu) - 1/G_0^{(1)}(\nu) \sim (U - U_0)^{\eta^*}$, i.e., where the crossing between $G_0^{(1)}$ and $G_0^{(2)}$ is governed by the minimal exponent η^* .

For the red crossings $\eta^* = 1$, i.e., we observe a linear crossing at one (positive and negative) Matsubara fre-

quency $\pm\nu^*$ while our numerical data indicate $\eta_\nu = 2$ for all other $\nu \neq \nu^*$. This is indeed consistent with the divergence of $\Gamma_c^{\nu\nu'(\omega=0)}$ at $\nu, \nu' = \nu^*$ observed in Ref. 4.

On the contrary, for the orange line the crossing between $G_0^{(1)}$ and $G_0^{(2)}$ happens, at the lowest order, in the same way for *all* Matsubara frequencies ν , i.e. $\eta_\nu = \eta^*$ (~ 0.5 according to our numerical data) for all ν . To see this, one should consider separately the behavior of both $\text{Re } G_0$ and $\text{Im } G_0$, as shown in the lower panel of Fig. 1 (left and right, respectively). In particular, one observes that on the left side of the crossing ($U < U_0$) $\text{Re } G_0$ displays the leading (square-root) behavior, while $\text{Im } G_0$ shows a linear (subleading) behavior for the first Matsubara frequency. On the right side after the crossing ($U > U_0$), $\text{Re } G_0 = 0$, and the leading (square-root) behavior appears for $\text{Im } G_0$ at all frequencies. Correspondingly, according to Eq. (5), $V(\nu) \neq 0$ for all frequencies which corresponds to a global divergence of Γ_c .

¹ T. Schäfer, G. Rohringer, O. Gunnarsson, S. Ciuchi, G. Sangiovanni, and A. Toschi, Phys. Rev. Lett. **110**, 246405 (2013).

² T. Schäfer, S. Ciuchi, M. Wallerberger, P. Thunström, O. Gunnarsson, G. Sangiovanni, G. Rohringer, and A. Toschi, Phys. Rev. B **94**, 235108 (2016).

³ M. Potthoff, Condens. Mat. Phys. **9**, 557 (2006).

⁴ Taking into account that, at the red crossings, the numerical data for $G_0^{(1)}$ and $G_0^{(2)}$ show that $G_0^{(2)}(\nu^*) - G_0^{(1)}(\nu^*) = -[G_0^{(2)}(-\nu^*) - G_0^{(1)}(-\nu^*)]$, the singularity in Γ_c originates from the fact that the two lines and two columns $\nu = \nu^*$ and $\nu' = \nu^*$, respectively, in χ_c are becoming equal (and, hence, the matrix χ_c becomes singular).